Detecting acute pain signals from human EEG

Guanghao Sun[1], Zhenfu Wen[1], Deborah Ok[2], Lisa Doan[2], Jing Wang[2,3,4,*], Zhe Sage Chen[1,3,4,*]

[1]Department of Psychiatry, New York University School of Medicine, New York, NY, United States
[2]Department of Anesthesiology, Perioperative Care, and pain Medicine, New York University School of Medicine, New York, NY, United States
[3]Department of Neuroscience and Physiology, New York University School of Medicine, New York, NY, United States
[4]The Neuroscience Institute, New York University School of Medicine, New York, NY, United States

*** Correspondence: jing.wang2@nyulangone.org (J.W.) or zhe.chen@nyulangone.org (Z.S.C.)**

ORCID 0000-0002-7615-1732 (G. Sun)

ORCID 0000-0002-7833-1753 (L. Doan)

ORCID 0000-0003-1580-1356 (J. Wang)

ORCID 0000-0002-6483-6056 (Z. S. Chen)

Number of figures and Table: 7 and 2

Keywords: State-space model; source localization; event-related potential; acute pain

Highlights

- Unsupervised learning detects the onset of acute pain signals.
- Source localization identifies regions of interest to improve detection accuracy.
- Cross-subject and cross-modality prediction of acute pain signals is feasible.

Abstract

Background: Advances in human neuroimaging has enabled us to study functional connections among various brain regions in pain states. Despite a wealth of studies at high anatomic resolution, the exact neural signals for the timing of pain remains little known. Identifying the onset of pain signals from distributed cortical circuits may reveal the temporal dynamics of pain responses and subsequently provide important feedback for closed-loop neuromodulation for pain.

New method: Here we developed an unsupervised learning method for sequential detection of acute pain signals based on multichannel human EEG recordings. Following EEG source localization, we used a state-space model (SSM) to detect the onset of acute pain signals based on the localized regions of interest (ROIs).

Results: We validated the SSM-based detection strategy using two human EEG datasets, including one public EEG recordings of 50 subjects. We found that the detection accuracy

varied across tested subjects and detection methods. We also demonstrated the feasibility for cross-subject and cross-modality prediction of detecting the acute pain signals.
Comparison with existing methods: In contrast to the batch supervised learning analysis based on a support vector machine (SVM) classifier, the unsupervised learning method requires fewer number of training trials in the online experiment, and shows comparable or improved performance than the supervised method.
Conclusions: Our unsupervised SSM-based method combined with EEG source localization showed robust performance in detecting the onset of acute pain signals.

1. Introduction

Pain is a highly dynamic process, and is constantly shaped by sensory inputs and internal affective or cognitive variables (Kucyi and Davis, 2017). A distributed network of cortical circuits, rather than a single "pain cortex", regulates pain (Apkarian et al., 2005; Perl, 2007). Human neuroimaging studies have advanced the understanding of brain mechanisms in pain. Studies using functional magnetic resonance imaging (fMRI) and positron emission tomography (PET) have identified regions involved in affective and sensory processing of acute pain, including the primary somatosensory cortex (S1), anterior cingulate cortex (ACC), and insular cortex (Hutchison et al., 1999; Isnard et al., 2011; Downar et al., 2003; Vierck et al., 2013; Liberati et al., 2018; van der Miesen et al., 2019; Mouraux and Iannetti, 2018). However, despite high spatial resolution, fMRI and PET cannot measure brain activity directly, and have limited temporal resolution (Wager et al., 2013). This lack of temporal specificity in fMRI or PET data makes it difficult to fully capture the dynamic nature of pain perception and experience. Meanwhile, non-invasive electroencephalography (EEG) has several significant advantages compared to other imaging modalities. First, EEG provides high temporal resolution and allows the assessment of oscillatory activity related to pain processing (Ploner et al., 2017). Studies have shown that acute pain triggers evoked potentials (or event-related potentials, ERPs) in the EEG, as well as elevated EEG theta and gamma powers (e.g., Stern et al., 2006; Ploner et al., 2017; Liberati et al., 2018; May et al., 2019). Second, EEG is portable, easy to apply, and cost-effective, which is appealing for future clinical applications. In scalp EEG recordings, the issue of volume conduction arises because the recording electrical potentials are distant from their source generator (Holsheimer and Feenstra, 1977). In order to understand the relationship between EEG and the underlying primary source configuration, the electrical conduction properties of the human head (the volume conductor) need to be modeled. Recent development in source localization has improved the spatial resolution for high-density EEG studies and enabled the examination of EEG biomarkers for the diagnosis and prognosis of pain and other neuropsychiatric disorders (Mouraux and Iannetti, 2018; David et al., 2020).

To date, several statistical methods have been developed for decoding the subjective pain or classifying the pain stimulus intensity for human subjects, based on either EEG signal alone (Schulz et al., 2012; Huang et al., 2013), or EEG combined with other neural or physiological signals (Tu et al., 2016; Lancaster et al., 2017). However, most of EEG-based pain studies have focused on (supervised) classification, which requires labeled data and many experimental trials used for model training. Such requirement may restrict its use for clinical applications where the number of trials are limited. In addition, nearly all EEG-based pain

detection or classification methods have used scalp EEG recordings directly in the sensor space, and few have analyzed the source signals. However, examination of the source-localized signals may reveal important cortical circuit mechanisms on pain processing. Recently, Tayeb et al. (2020) combined EEG source localization and machine learning techniques to decode pain perception for a real-time reflex system in prosthesis in a single-subject case study. More systematical investigation for using source localization to study pain signals are urgently needed to improve our understanding of central pain mechanisms and to enable future neuroengineering strategies for diagnosing and treating pain.

In our prior work, we have developed several methods to detect acute pain signals in freely behaving rodents based on recorded spikes or local field potentials (LFPs), and these approaches can be adapted to EEG signals (Chen and Wang, 2016; Chen et al., 2017; Hu et al., 2018; Zhang et al., 2018; Xiao et al., 2019). However, in contrast to the rodent LFPs, scalp EEG recordings have lower signal-to-noise ratio (SNR), and are subject to various sources of artefacts, including eye blinks and motor movement, which pose a great challenge for sequential detection. Here, we aim to achieve three goals in this study. First, we integrate EEG source localization and machine learning to detect acute pain signals using a public human EEG dataset with 50 healthy subjects (Tiemann et al., 2018), and extend this investigation to an additional independent EEG recording of two patients with chronic back pain. Second, based on source localization, we study the amplitude and latency of region-specific bilateral ERPs. Finally, we propose an unsupervised learning method for detecting the onset of acute pain signal using a state-space model (SSM), and validate this method in a sequential (pseudo online) pain detection manner. As a complementary approach, we also compare the performance between unsupervised learning and supervised learning methods.

2. Materials and Methods

2.1 Experimental data

Public dataset. The first human EEG dataset was obtained from a published study (Tiemann et al., 2018), in which data were collected in Germany and then in made in public (https://osf.io/bsv86/). Fifty-one right-handed healthy participants (25 females) with a mean age of 27 years (range 20-37) participated in the study. Participants were recruited via advertisements on bulletin boards of local universities. The study was approved by the local ethics committee and carried out in accordance with the relevant guidelines and regulations. The detailed protocol is referred to (Tiemann et al., 2018).

Briefly, the experiment included three core conditions (motor, perceptual and autonomic), which were presented in randomized order. In each condition, 60 painful stimuli were applied to the dorsum of the left hand. We have focused on the motor condition (with 50 participated subjects) in our current study. Stimulus intensity was varied between three individually adjusted levels (Leve-1 [$n = 20$], Level-2 [$n = 20$], and Level-3 [$n = 20$]) in a pseudorandomized sequence. Painful stimuli were applied by means of cutaneous laser stimulation (160 nm wavelength, 1-ms pulse duration, 5-mm spot diameter), which induces a pinprick-like sensation. Stimulation sites were slightly changed after each stimulation to avoid tissue damage and habituation/sensitization effects. In the motor condition, reaction times (RTs) were measured in the millisecond range. Subjects were instructed to close eyes during the course of experiment. Here we focused on the classification between Level-3 and Level-1 trials.

EEG data were recorded with 65 scalp electrodes consisting of all electrodes of the International 10-20 system (**Fig. 1A**). Two additional electrodes were fixed below the outer canthus of each eye. During the recording, the EEG was referenced to the FCz electrode, grounded at AFz, sampled at 1000 Hz, high-pass filtered at 0.015 Hz, and low-pass filtered at 250 Hz. EEG data were preprocessed using the BrainVision Analyzer software (Brain Products, Munich, Germany) and then downsampled to 500 Hz. For artifact detection, a high-pass filter of 1 and a 50 Hz notch filter for line noise removal were applied to the EEG data. Independent component analysis (ICA) was performed to identify components representing eye movements and muscle artifacts based on the energy at spatial topographic map (**Fig. 1B**).

Chronic pain patient dataset. In the second EEG dataset, 32-channel EEG recordings (Enobio, Neuroelectrics) were collected (sampling rate: 500 Hz; high-pass filtered at 0.1 Hz, and low-pass filtered at 250 Hz) at the NYU Langone Health Comprehensive Epilepsy Center. The study was performed in accordance with the National Institutes of Health (NIH) policy for human subjects, and were approved by the Institutional Review Board (IRB) at the NYU School of Medicine. Two right-handed subjects (ages: 69 and 48, female and male, respectively) with chronic back pain first underwent resting EEG with eyes closed and eyes open for 5 minutes each. The testing protocol consisted of 40 trials of mechanical stimulation (noxious painful pinprick (PP) with a 32 gauge blunt needle vs non-noxious stimulus (NP) with a 10 g monofilament) on the right hand, followed by another 40 trials of mechanical stimulation to the lower back. In both cases, noxious and non-noxious stimulations were randomly interleaved with an inter-stimulus interval of 8-12 sec. Numerical rating scale (NRS; 0-10) statistics in each condition were summarized in **Table 1**. Subjects were instructed to keep the eyes open while looking away to minimize or avoid anticipation.

Table 1. Mean numeric rating scale (NRS) statistics for two chronic pain patients. The numbers in the bracket show the (median, IQR) statistics.

Subject	NRS with PP to hand	NRS with NP to hand	NRS with PP to back	NRS with NP to back
Subject #1	1 (1, 1)	1 (1, 1)	1.5 (1, 2)	1 (1, 1)
Subject #2	3 (2, 4)	2 (1, 2)	4 (3, 5)	2 (2, 3)

2.2 EEG source localization

We conducted the source localization to reconstruct the dipole activity at the cortical surface (**Fig. 1C**). Specifically, we used a mean head model and employed the established MNE software package (Gramfort et al., 2013; https://mne.tools/stable/index.html). All EEG data were down-sampled to 500 Hz, notch filtered to remove 50 Hz line noise and its harmonic, and high-pass filtered (>0.1 Hz) using a zero-phase finite impulse response filter. Bad channels were automatically detected and repaired with the Autoreject toolbox (Jas et al., 2017). Muscle and ocular artifacts were identified by using ICA, and the components deemed as artifacts were excluded.

We extracted the time series of cortical EEG sources using the dynamic statistical parametric mapping (dSPM) method (Dale et al., 2000), which was implemented in the MNE software package. Individual noise covariance matrix was estimated using all preprocessed EEG data. A linear collocation single-layer boundary-element method (BEM) was used to compute the forward solution that models the

generated signal pattern at each dipole. The forward solution is expressed as the leadfield matrix, where each column corresponds with the potential or field distributions on all sensor for one of the (x,y,z)-orientations of the dipole. We computed the leadfield matrix for each voxel using a realistically shaped three-shell boundary-element volume conduction model based on the template of Montreal Neurological Institute (MNI) brain because no structural MRI was collected for these participants. We further extracted time series of brain regions defined by the Desikan-Killiany Atlas (Desikan et al., 2006).

Among a total of 4098×2=8196 dipoles considered in two hemispheres, we selected several regions of interest (ROIs): precentral gyrus, postcentral gyrus, ACC, insula, from both left and right hemispheres, totaling 8 ROIs. Notably, the postcentral gyrus is the location of the S1, whereas the precentral gyrus is the anatomical location of the primary motor cortex (M1).

2.3 Spectrum analysis

Multitapered spectral analyses for EEG spectrum or spectrogram were performed using the Chronux toolbox (chronux.org). Specifically, we chose a half-bandwidth parameter W such that the windowing functions were maximally concentrated within $[-W, W]$. We chose $W > 1/T$ (where T denotes the duration) such that the Slepian taper functions were well concentrated in frequency and had bias reducing characteristics. In terms of Chronux function setup, we used the tapers setup $[TW, N]$, where TW is the time-bandwidth product, and $N = 2 \times TW-1$ is the number of tapers. Since the taper functions are mutually orthogonal, they give independent spectral estimates. In time-frequency analyses, we used a moving window length of 250 ms and a step size of 50 ms. We used $TW = 5$ in computing the spectrum and spectrogram. From the spectrogram, we computed the Z-scored spectrogram, where the baseline was defined as the 2-s period prior to the stimulus onset.

2.4 State-space analysis

We formulated the problem of detecting the onset of acute pain signals as a change-point detection problem (Chen et al., 2017; Hu et al., 2018), in the context of state-space analysis (Chen, 2015). The SSM consists of a state equation and a measurement equation. In the state equation, we assumed that the EEG-derived activity at the k-th time index, represented by a C-dimensional vector $\boldsymbol{y}_k$, was driven by a one-dimensional latent Markovian process z_k:

$$z_k = az_{k-1} + \epsilon_k$$

where ϵ_k specifies a temporal Gaussian prior (with zero mean and variance σ^2) on the latent process, $0<|a|<1$ denotes the first-order autoregressive (AR) coefficient. In the measurement equation, we assumed that the measurement $\boldsymbol{y}_k$ followed a linear dynamical system

$$\boldsymbol{y}_k = \boldsymbol{c}z_k + \boldsymbol{d} + \boldsymbol{v}$$

where $\boldsymbol{d}$ denotes a DC constant, and $\boldsymbol{v}$ denotes the uncorrelated Gaussian noise with zero mean and covariance matrix $\boldsymbol{\Sigma}$. In our unsupervised detection strategy, $\boldsymbol{y}_k$ corresponded to the time-averaged band-passed filtered (1-100 Hz) EEG amplitude within the k-th time bin (bin size: 100 ms).

2.5 Model identification and online change-point detection

Let Θ denote all unknown model parameters, we have developed an iterative expectation-maximization (EM) algorithm to estimate latent state sequences (E-step) and unknown parameters $\Theta=\{a, \boldsymbol{c}, \boldsymbol{d}, \sigma^2, \boldsymbol{\Sigma}\}$ (M-step). Details of this estimation procedure is referred to (Chen et al., 2015). When the observations are demeaned, we set $\boldsymbol{d}=\boldsymbol{0}$.

In an online filtering operation, we used the Kalman filter to estimate the predicted latent state. The Kalman filter equations are given as follows (Haykin, 2014):

$$\hat{z}_{k|k-1} = a\hat{z}_{k-1|k-1}$$
$$Q_{k|k-1} = a^2 Q_{k-1|k-1} + \sigma^2$$
$$\hat{\boldsymbol{y}}_{k|k-1} = \boldsymbol{c}\hat{z}_{k-1|k-1} + \boldsymbol{d}$$
$$\boldsymbol{G}_k = Q_{k|k-1}\boldsymbol{c}^T(Q_{k|k-1}\boldsymbol{c}\boldsymbol{c}^T + \boldsymbol{\Sigma})^{-1}$$
$$\hat{z}_{k|k} = \hat{z}_{k|k-1} + \boldsymbol{G}_k(\boldsymbol{y}_k - \hat{\boldsymbol{y}}_{k|k-1})$$
$$Q_{k|k} = Q_{k|k-1}(1 - \boldsymbol{G}_k\boldsymbol{c})$$

From the online latent state estimate $\hat{z}_{k|k}$, we computed the Z-score related to the baseline: $\mathrm{Z\_score} = \frac{z-\mathrm{mean}(z_{\mathrm{baseline}})}{\mathrm{SD}(z_{\mathrm{baseline}})}$ and further converted it to the one-tailed *p*-value (Chen and Wang, 2016; Chen et al., 2017). In the training trial for model identification, the baseline was defined by the pre-stimulus 5-s period before the stimulus onset. For the sequential detection setting, the baseline was computed as the median statistic within the total testing periods while excluding the outliers outside the range of three-fold SD.

We monitored the time-varying Z-score to assess the significance of change point detection. The significance criterion of Z-score change was determined by a critical threshold. For instance, using 95% significance level, it was concluded that when Z-score−CI > 1.65 or Z-score + CI < −1.65, where the CI denotes the confidence interval derived from the state posterior variance.

To assess the detection sensitivity and specificity, we computed the ROC (receiver operating characteristic) curve, and the area under curve (AUC) indicates the overall detection performance (1 being perfect, 0.5 being a chance level). The ROC plot shows the tradeoff of sensitivity and specificity at different thresholds.

2.6 Support vector machine (SVM) classifier

SVM is a discriminative classifier that constructs the classification boundary by a separating hyperplane with maximum margin. Specifically, SVM maps the high-dimensional input $\boldsymbol{y}_i$ ($i = 1,\ldots, N$, where N denotes the training sample size) into a high-dimensional feature space and maximizes the margin from the hyperplane to the origin. Here we used a linear kernel for binary classification, and trained the linear SVM with the sequential minimal optimization (SMO) algorithm (Fan et al., 2005) (libsvm MATLAB package: https://www.csie.ntu.edu.tw/~cjlin/libsvm/). The SVM's performance was insensitive to the choice of hyperparameter. The features used in the SVM were specific power at three frequency bands (4-12 Hz, 12-45 Hz, 60-100 Hz). We employed an accumulative decoding strategy by accumulating the features in time (Zhang et al., 2018). If the dimensionality of features at the first temporal bin (bin size: 100 ms) was L, then the dimensionality at the second time bin would become $2L$, and so on.

For binary classification, let n_1 and n_2 denote the number of trials recorded under two different conditions, we split the total (n_1+ n_2) trials into two groups, 80% used for training, and 20% used for testing. We conducted 5-fold cross-validation and then computed the average test accuracy. We randomized the

trial order and repeated the cross-validation procedure 100 times, and reported the mean ± S.E.M. decoding accuracy from all Monte Carlo experiments as the final performance. By default, the classification threshold was 0.5. We further varied the classification threshold and computed the AUC.

As a control, we also computed the chance-level decoding accuracy and AUC. We randomly permuted class labels between two classes and repeated the decoding analysis. This shuffling procedure was repeated 500 times, and we reported the chance level by the averaged classification accuracy based on shuffled data with permuted labels. The chance-level accuracy (or AUC) should be close to 50% (or 0.5) when the sample sizes from both classes are perfectly balanced.

2.7 ROI selection

A naïve approach was to select all eight ROIs as the features in decoding analysis. However, we found that this strategy was not optimal. Instead, we used two alternative strategies in our investigation. The first strategy was to customize the selection for each subject, and find the best ROI combination to optimize the performance. The second strategy was to impose a common ROI selection for all subjects and select suboptimal features (via exhaustive combinatorial search) to optimize the overall group performance. We implemented both strategies and reported their results separately.

2.8 Statistics

Nonparametric statistical tests were used to assess the statistical significance based on the significance level of $p<0.05$. All data analyses reported below were conducted in Python or MATLAB. Custom software will be distributed online (www.cn3lab.org/software).

3. Results

3.1 Source localized ERPs

Upon EEG data preprocessing via independent component analysis (ICA), we performed EEG source localization (**Fig. 1**; **Methods**). We identified eight regions of interest (ROIs) from two hemispheres: precentral gyrus (M1), postcentral gyrus (S1), ACC, and insula.

In the first EEG dataset, after source localization, we identified the single-trial ERPs from each ROI (**Fig. 2A**). Due to a lower SNR in single trials, we also computed the averaged ERPs by aligning them with their peaks (**Fig. 2B**). Among a subset of 50 subjects (18/50), we did not observe clear ERPs at both single-trial and averaging-trial levels; and we labeled these subjects and associated data as Group 1, and the remaining 32 subjects with clear ERPs as Group 2.

For Group 2, we compared the peak ERP latency between different ROIs from both hemispheres, and found that there was a significant latency gap between the ACC and M1 ($p=1.2\times10^{-5}$, rank-sum test), between the S1 and M1 ($p=0.02$), and between the ACC and insular ($p=5\times10^{-4}$) at the contralateral site of the simulated hand, but no significant difference in latency between any pair at the ipsilateral side (**Fig. 2C**). The population statistics showed

that the ERPs occurred at the ACC and S1 first (statistically insignificant between the S1 and ACC ERP latencies, p=0.08), followed by the M1 and the insular.

3.2 Sequential detection results from the unsupervised method

To simulate the online detection experimental setup, we used the first Level-3 (high intensity pain) trial to estimate the SSM, and tested the remaining Level-3 and all Level-1 trials in a sequential manner (**Fig. 3A,B**). The sensitivity was computed based on the true positive (TP) rate from the Level-3 trials, whereas the specificity was computed based on the false positive (FP) rate from the Level-1 trials. We varied the detection threshold and computed the ROC curve and AUC statistic (**Fig. 3C**). At the single trial level, there was a weak yet non-significant correlation (ρ=0.29, p=0.06, Spearman's rank correlation) between the detection latency and subject's RT (**Fig. 3D**). In addition, the detection latency from Level-3 trials (median: 180 ms) was significantly shorter than the detection latency from Level-1 trials (median: 202 ms) by pulling all successfully detected trials among all subjects ($p=1.5\times10^{-5}$, rank-sum test). At the population level, we compared the detection performance between Group 1 and Group 2, and found that the AUC statistics was significantly higher in Group 2 than in Group 1 ($p=1.9\times10^{-5}$; rank-sum test**; Fig. 3E**). The same trend remained significant when we allowed custom feature selection for each subject ($p=3.4\times10^{-5}$; **Fig. 3F**). As expected, the AUC statistics from both groups were improved when custom features are optimized for each subject.

It is noted that Level-1 trials were not the true negative controls (i.e., non-painful trials), therefore the difficulty for distinguishing high from low-intensity pain stimuli was presumably greater than distinguishing painful from non-painful stimuli.

3.3 Cross-subject prediction

Furthermore, we tested the generalization ability of the proposed unsupervised learning method across subjects (n=32, within Group 2). Specifically, we selected 7 trained models from "good" subjects who achieved >0.7 AUC statistic in detection, and ran the testing on the remaining subjects. We found that most trained models achieved reasonably good cross-subject prediction results as compared to within-subject prediction (**Fig. 4A**). Notably, the best model predicted 16 subjects (AUC>0.65) and achieved averaged AUC of 0.62 (**Fig. 4B**), comparable to the baseline (i.e., within-subject prediction, averaged AUC of 0.64). These results suggest that given a good trained model, we can achieve comparable results between cross-subject and within-subject prediction.

3.4 Batch classification results from the supervised method

As a comparison, we ran supervised decoding analysis using a linear SVM and reported the classification accuracy between Level-3 and Leve-1 trials. We observed a difference in Z-score spectrogram between two levels at the trial-averaged level (**Fig. 5A**). However, there was a high degree of variability at the single-trial level. We have compared the temporal and spectral features, and found that the spectral features yielded slightly yet consistently better results than temporal features. In addition, combining temporal and spectral features together did not show

significantly improved performance. Therefore, to avoid overfitting, we have only used spectral features in SVM training.

At the single-subject level, we computed the cumulative cross-validated decoding accuracy curve and AUC statistic (**Fig. 5B**), where the timing of these performance peak values indicated the moment that selected EEG features showed the maximum discriminability. At the group level, we assumed the use of common ROIs and spectral features across all subjects, and reported the peak accuracy (based on 0.5 threshold) and peak AUC statistic. The peak accuracy and peak AUC derived from SVM were positively correlated (Pearson's correlation ρ=0.71, p=10^{-5}; **Fig. 5C**). However, the AUC results obtained from unsupervised SSM and supervised SVM methods were not correlated (Pearson's correlation ρ=0.08, p=0.56; **Fig. 5D**). We further compared the classification performance between Group 1 and Group 2, and found significant difference between groups in peak accuracy (p=1.2×10^{-4}, rank-sum test), but not in AUC (**Fig. 5E**).

3.5 Results on the second dataset

Next, for a demonstration purpose, we repeated the same analysis pipeline for two patients with chronic back pain from the second EEG dataset. The only difference in settings was that we compared painful stimulations with true negative (non-noxious stimuli) controls. In addition, we compared the decoding results based on hand or back stimulations, in both unsupervised and supervised learning settings. Selected results are shown in **Fig. 6**. Specifically, we found that the AUC statistic derived from the unsupervised method was better in hand than back stimulations, and the performance from the SVM classification was better in back than hand stimulations (**Table 2**). It should be noted that these results were obtained based on using the same features across two subjects (which were also consistent with the features used in the analysis of the first EEG dataset); when customized (either ROI or spectral bands) feature selection was allowed for individual subjects, the results could be further improved.

Table 2. Results of cross-modality and cross-subject acute pain detection. In the supervised learning method, the accuracy was derived based on the 0.5 threshold used in binary classification.

Training	Testing	Unsupervised	Supervised	
		AUC	Peak AUC	Peak accuracy
Hand (#1)	Hand (#1)	0.81	0.74	0.61
	Back (#1)	0.61	0.58	0.55
	Hand (#2)	0.70	0.50	0.50
	Back (#2)	0.73	0.71	0.73
Back (#1)	Hand (#1)	0.80	0.58	0.70
	Back (#1)	0.65	0.83	0.66
	Hand (#2)	0.70	0.46	0.52
	Back (#2)	0.73	0.45	0.53
Hand (#2)	Hand (#1)	0.79	0.62	0.63
	Back (#1)	0.60	0.59	0.58
	Hand (#2)	0.71	0.77	0.67

	Back (#2)	0.70	0.59	0.62
Back (#2)	Hand (#1)	0.80	0.68	0.65
	Back (#1)	0.61	0.43	0.53
	Hand (#2)	0.72	0.57	0.55
	Back (#2)	0.71	0.73	0.60
Mean		**0.71**	**0.61**	**0.60**

To test cross-modality prediction in each subject, we trained the trials from hand stimulations and tested the trials from back stimulations, and vice versa. Furthermore, we tested cross-subject prediction by training the trials from subject #1 and tested the trials from subject #2, and vice versa. All results are summarized in **Table 2**. Notably, the AUC statistics varied from 0.60 to 0.81 based on our unsupervised sequential detection method, outperforming the SVM method (p=0.0113; signed rank test). This performance discrepancy was possibly due to the fact that the SVM classifier was sensitive to feature calibration, whereas the SSM aimed to detect the "change-points", which was more robust across trials, modalities and subjects (specifically, the SSM was trained on 1 trial and tested on $40\times2\times2=160$ trials). Although our results were obtained from two subjects, this preliminary result suggested the feasibility for cross-modality and cross-subject prediction in acute pain.

3.6 Comparison of results without source localization

Next, to investigate the benefit of source localization, we compared SVM classification results with and without source localization, and illustrated this point using two subjects from the second EEG dataset. Since the number of channels were relatively large compared to the number of trials, we resorted to dimensionality reduction. Specifically, to match the same feature dimensionality as in source localization, we conducted principal component analysis (PCA) and kept the number of principal components roughly the same as the number of selected ROIs. Under the same setting, the SVM performance with source localization was better (**Fig. 7A**). In the unsupervised sequential detection setting, the AUC statistic without source localization was worse than that with source localization (**Fig. 7B**). Together, these results pointed to improved performance in acute pain detection for both supervised and unsupervised methods.

4. Discussion and Conclusion

4.1 Relation to other work

We have developed an unsupervised learning method for detection of acute pain signals based on source localized EEG signals. In our detection procedure, the SSM parameters were identified based on the first trial, then the model was used to test the remaining trials in a sequential manner. In contrast, most pain decoding methods are based on batch supervised learning without source localization. In a few studies (Huang et al., 2013; Lancaster et al., 2017), the reported accuracy was 70-86% for detecting the pain stimulus intensity and 77-86% for

detecting the subjective pain score (Schulz et al., 2012; Tu et al., 2016). See (van der Milesen et al., 2019) for a review on this topic. Among the total 52 examined subjects, our best 5-fold cross-validated detection accuracy for a single subject was 76%; the best AUC statistic was 0.79 (unsupervised) and 0.95 (supervised)---all results would be further improved if we allowed custom optimization for each subject. The discrepancy from our results and the literature could be due to the difference in experimental protocols, stimuli, assessment criteria (e.g., 5-fold vs. 10-fold cross-validation) and subject variability. This is especially the case when the number of tested subjects is large here, and we have restricted ourselves to using the same features across all subjects. Therefore, subject variability poses an issue for cross-subject prediction. In addition, supervised learning is often limited by a small number of training trials available in pain experiments, raising the issue of potential overfitting.

In a single-subject EEG case study, Tayeb et al. (2020) localized the cortical sources and observed early strong ACC activation corresponding to the noxious stimulus condition. Moreover, activation of the posterior cingulate cortex (PCC) was observed during noxious stimulations. To classify innocuous, moderately more intense, and noxious stimulations of the amputee's phantom lib using transcutaneous nerve stimulation (TENS), they reported a test accuracy of 94.6% for the single subject. Since TENS was used as a intervention to reduce hyperalgesia for pain control in their study, it is difficult to directly compare their results with ours.

In our investigations, we found that a subset (18/50) of subjects from the first dataset did not show clear ERPs at the cortical surfaces upon EEG source localization. This could be due to multiple reasons: First, we have witnessed very strong alpha rhythms in all EEG channels due to eye closure of all participants during the pain experiment. Band-stop filtering was not able to completely eliminate the influence of this alpha dominance. This effect has also been confirmed in previous Granger causality analyses (Ploner et al., 2009; Guo et al., 2000), when we attempted to estimate the directed information flow between ROIs (results not shown). Second, there were potentially other uncorrected artefacts beyond eye blinks that couldn't be removed from the ICA method. Finally, the accuracy of source localization can be further improved using higher-density EEG recordings and a more accurate head model.

4.2 Feature selection

Selection of features, including spatial (ROIs) and spectral domains, is very important for both unsupervised and supervised detection methods. Among the 4×2 ROIs that were examined in two datasets, we found that the S1 from both hemispheres, and the ACC and insula from the contralateral hemisphere, were the most discriminating features at the group level. However, when we allowed custom subject optimization, the choice of ROIs had a high degree of variability. Due to the limited number of trials, we have tried to reduce the number of features to reduce the risk of overfitting. With the development of increasingly precise EEG source localization, inclusion of additional cortical or subcortical ROIs that are specific for pain processing can potentially improve the detection performance. However, improved EEG source localization would jointly depend on high-density EEG recordings and a more accurate head model based on structural MRI specified for each subject.

In terms of spectral features, multiple lines of work in humans and rodents have shown that theta and gamma-band oscillations at the prefrontal and S1 regions can encode pain percept (Sarnthein et al. 2006; Schulz et al., 2015; Ploner et al., 2017; May et al., 2019; Zhang et al., 2018; Zhou et al., 2018; Tan et al., 2019). While theta oscillations can be corrupted by potential low-frequency artifacts, gamma-band power are usually more robust. In the time domain, the ERPs appear to be the most salient feature, which are visible in both the sensor and source spaces. However, it was possible that ERPs only represent an indirect readout of the function of the nociceptive system (Iannetti et al., 2008; Mouraux and Iannetti, 2009), in that the stimulus-evoked ERPs are not determined by pain perception per se, but are mainly determined by the saliency of eliciting nociceptive stimuli. Since the high-intensity stimuli are more salient than low-intensity stimuli, the detection methods alone cannot distinguish whether the classification performance is based on stimulus saliency or on some other feature related to pain (Senkowski et al., 2014). Future experimental designs that account for the saliency effect or combine EEG with fMRI recordings may help disambiguate such confound (Zhang et al., 2020).

4.3 Challenges and future directions

In most human pain experiments, subjects were instructed to sit still and close their eyes. Thus, it remains a challenging task to translate findings from these highly structured studies to freely moving subjects. Furthermore, pain detection analyses in clinical applications can be improved by the development of online artifact rejection methods. To accommodate real-time EEG processing, online ICA and source localization may be considered (Pion-Tonachii et al., 2015). In addition, it may be difficult to distinguish pain from pain anticipation based on the ERP alone (Huang et al., 2017; Ploghaus et al., 1999), since pain anticipation can also induce change in neural responses (Babiloni et al., 2008; Urien et al., 2018). Strategies that combine temporal change-point detection with analyses of other frequency-specific features can potentially provide such distinction.

EEG recordings often lasted a long period of time during the course of experiment, raising the issue of data non-stationarity. In our unsupervised pain detection strategy, we have assumed the model stationarity across the testing trials. To our surprise, the SSM has demonstrated a good level of robustness in the presence of data non-stationarity, as the model was estimated based on the first trial and tested on all remaining trials. To accommodate sequential detection tasks at a longer timescale, we may introduce online model adaptation, so that the baseline and model parameters are updated on a regular basis. Furthermore, the SSM-based detection strategy has shown great potential in cross-modality and cross-subject prediction of acute pain signals. Further investigations are required to extensively test more human subjects in pain experiments without eye closure. Although our decoding study is presented to EEG analysis, our approach is equally applicable to magnetoencephalography (MEG) data analysis (e.g., Kisler et al., 2020).

Another important research direction is to extend the detection of acute pain to experimental tonic pain (e.g., Schultz et al., 2015; May et al., 2019; Nickel et al., 2020). In our prior work in

rodent models, we have developed methods to detect tonic pain based on neuronal spiking activity and/or LFPs based on a supervised SVM classifier (Xiao et al., 2019), or an unsupervised SSM-based strategy (Zhang et al., 2020). Development of a similar analysis pipeline for human patients experiencing with tonic pain may further enhance our understanding of central pain mechanism.

In summary, we have developed an unsupervised learning EEG analysis paradigm to decode the onset of acute pain. Future development of high-density EEG-based decoding strategies for acute or chronic pain can ultimately advance human pain studies and diagnosis.

Author contribution statement

Guanghao Sun: Formal analysis, Investigation, Methodology, Software, Visualization. **Zhenfu Wen:** Data analysis, Software. **Deborah Ok**: Data collection, Data curation. **Lisa Duan**: Data curation. **Jing Wang:** Conceptualization, Funding acquisition, Writing – review & editing. **Zhe Sage Chen**: Conceptualization, Funding acquisition, Methodology, Resources, Supervision, Writing – original draft, Writing – review & editing.

Declaration of Competing Interests

The authors declare no competing interests.

Acknowledgments

We thank Dr. Markus Ploner for sharing the first human EEG dataset. This work was partially supported by the US National Science Foundation (NSF) grant CBET-1835000 (ZSC, JW), NIH grants R01-NS100065 (ZSC, JW), R01-MH118928 (ZSC), and the NYU Interdisciplinary Pain Program (JW, LD).

References

Apkarian AV, Bushnell MC, Treede R-D, Zubieta J-K. (2005). Human brain mechanisms of pain perception and regulation in health and disease. *Pain* 9: 463-484.

Babiloni C, *et al*. (2008). Cortical alpha rhythms are related to the anticipation of sensorimotor interaction between painful stimuli and movement: a high-resolution EEG study. *J. Pain* 9: 902-911.

Chen Z, editor (2015). *Advanced State Space Methods for Neural and Clinical Data*. Cambridge Univ. Press.

Chen Z, Wang J (2016). Statistical analysis of neuronal population codes for encoding acute pain. *Proc. IEEE ICASSP*, pp. 829-833, doi: 10.1109/ICASSP.2016.7471791.

Chen Z, Zhang Q, Tong APS, Manders TR, Wang J (2017). Deciphering neuronal population codes for acute thermal pain. *J. Neural Eng.* 14: 036023.

Dale AM, *et al.* (2000). Dynamic statistical parametric mapping: combining fMRI and MEG for high-resolution imaging of cortical activity. *Neuron* 26: 55-67.

Davis, K.D., Aghaeepour, N., Ahn, A.H. *et al.* (2020). Discovery and validation of biomarkers to aid the development of safe and effective pain therapeutics: challenges and opportunities. *Nat. Rev. Neurol.* 16: 381-400.

Desikan RS, *et al.* (2006). An automated labeling system for subdividing the human cerebral cortex on MRI scans into gyral based regions of interest. *Neuroimage* 31: 968-980.

Downar J, Mikulis DJ, Davis KD (2003). Neural correlates of the prolonged salience of painful stimulation. *Neuroimage* 20: 1540-1551.

Fan R-E, Chen P-H, Lin C-J (2005). Working set selection using second order information for training support vector machine. *J. Machine Learning Res*. 6: 1889-1918.

Gramfort A, *et al.* (2013). MEG and EEG data analysis with MNE-Python. *Front. Neurosci.* 7: 267.

Guo X, Zhang Q, Singh A, Wang J, Chen Z. (2020). Granger causality analysis for rat cortical functional connectivity in pain. *J. Neural Eng.* 17: 016050.

Haykin S (2014). *Adaptive Filter Theory* (5th edition). Pearson.

Holsheimer J, Feenstra BW (1977). Volume conduction and EEG measurements within the brain: A quantitative approach to the influence of electrical spread on the linear relationship of activity measured at different locations. *Electroencephalogr. Clin. Neurophysiol.* 43: 52-58.

Hu L, Iannetti GD (2016). Issues in pain prediction---beyond pain and gain. *Trends Neurosci.* 39: 640-642.

Hu S, Zhang Q, Wang J, Chen Z (2018). Real-time particle filtering and smoothing algorithms for detecting abrupt changes in neural ensemble spike activity. *J. Neurophysiol.* 119: 1394-1410.

Huang G, Xiao P, Hung YS, Iannetti GD, Zhang ZG, Hu L (2013). A novel approach to predict subjective pain perception from single-trial laser-evoked potentials. *Neuroimage* 81: 283-293.

Huang Y, Shang Q, Dai S, Ma Q (2017). Dread of uncertain pain: An event-related potential study. *PLoS ONE* 12(8): e0182489.

Hutchison WD, Davis KD, Lozano AM, Tasker RR, Dostrovsky JO (1999). Pain-related neurons in the human cingulate cortex. *Nat. Neurosci.* 2: 403-405.

Iannetti GD, Mouraux A (2010) From the neuromatrix to the pain matrix (and back). *Exp. Brain Res.,* 205: 1-12.

Iannetti GD, Hughes NP, Lee MC, Mouraux A (2008). Determinants of laser-evoked EEG responses: pain perception or stimulus saliency? *J. Neurophysiol*. 100: 815-828.

Isnard J, Magnin M, Jung J, Mauguiere F, Garcia-Larrea L (2011). Does the insula tell our brain that we are in pain? *Pain* 152: 946-951.

Jas M, *et al.* (2017). Autoreject: automated artifact rejection for MEG and EEG data. *Neuroimage* 159: 417-429.

Kisler LB, *et al*. (2020). Abnormal alpha band power in the dynamic pain connectome is a marker of chronic pain with a neuropathic component*. Neuroimage Clin*. 26: 102241.

Kucyi A, Davis KD (2017). The neural code for pain: from single-cell electrophysiology to the dynamic pain connectome. *Neuroscientist* 23: 397-414.

Lancaster J, Mano H, Callan D, Kawato M, Seymour B (2017). Decoding acute pain with combined EEG and physiological data. *Proc. IEEE/EMBS Conf. Neural Eng. (NER),* pp. 521-524, doi: 10.1109/NER.2017.8008404.

Lenz FA, Rios M, Zirh A, Chau D, Krauss G, Lesser RP (1998). Painful stimuli evoke potentials recorded over the human anterior cingulate gyrus. *J. Neurophysiol.* 79: 2231-2234.

Liberati G, Klocker A, Algoet M, Mulders D, Safronova MM, Ferrao Santos S, *et al.* (2018). Gamma-band oscillations preferential for nociception can be recorded in the human insula. *Cereb. Cortex* 28: 3650-3664.

Liberati G, Klocker A, Safronova MM, Ferrao Santos S, Ribeiro Vaz JG, Raftopoulos C, *et al.* (2016). Nociceptive local field potentials recorded from the human insula are not specific for nociception. *PLoS Biol.* 14: e1002345.

May ES, Nickel MM, et al. (2019). Prefrontal gamma oscillations reflect ongoing tonic back pain patients. *Hum. Brain Mapp*. 40: 293-305.

Mouraux A, Iannetti GD (2009). Nociceptive laser-evoked brain potentials do not reflect nociceptive-specific neural activity. *J. Neurophysiol.* 101: 3258-3269.

Mouraux A, Iannetti GD (2018). The search for pain biomarkers in the human brain, *Brain* 141: 3290-3307.

Nickel MM, Dinh ST, *et al.* (2020). Neural oscillations and connectivity characterizing the state of tonic experimental pain in humans. *Hum. Brain Mapp*. 41: 17-29.

Perl ER (2007). Ideas about pain, a historical view. *Nat. Rev. Neurosci.* 8: 71-80.

Pion-Tonachini L, Hsu S-H, Makeig S, Jung T-P, Cauwenberghs G. Real-time EEG source-mapping toolbox (REST): online ICA and source localization. *Proc. IEEE Eng. Med. Biol. Soc. (EMBC'15)*, pp. 4114-4117.

Ploghaus A, Tracey I, Gati JS, Clare S, Menon RS, Matthews PM, *et al.* (1999). Dissociating pain from its anticipation in the human brain. *Science* 284: 1979-1981.

Ploner M, Schoffelen J-M, Schnitzler A, Gross J (2009). Functional integration within the human pain system as revealed by Granger causality. *Hum. Brain Mapp*. 30: 4025-4032.

Ploner M, Sorg C, Gross J (2017). Brian rhythms of pain. *Trends Cog. Sci.* 21: 100-110.

Rainville P, Duncan GH, Price DD, Carrier B, Bushnell MC (1997). Pain affect encoded in human anterior cingulate but not somatosensory cortex. *Science* 277: 968-971.

Sarnthein J, Stern J, Aufenberg C, Rousson V, Jeanmonod D (2006). Increased EEG power and slowed dominant frequency in patients with neurogenic pain, *Brain* 129: 55-64.

Schulz E, Zherdin A, Tiemann L, Plant C, Ploner M (2012). Decoding an individual's sensitivity to pain from the multivariate analysis of EEG data. *Cereb. Cortex* 22: 118-123.

Schulz E, May ES, Postorino M, Tiemann L, Nickel MM, Witkovsky V, Schmidt P, Gross J, Ploner M (2015). Prefrontal gamma oscillations encode tonic pain in humans. *Cereb, Cortex* 25: 4407-4414.

Senkowski D, Höfle M, Engel AK. (2014) Crossmodal shaping of pain: A multisensory approach to nociception. *Trends Cogn. Sci.*, 18, 319-327.

Stern J, Jeanmonod D, Sarnthein J (2006). Persistent EEG overactivation in the cortical pain matrix of neurogenic pain patients. *Neuroimage* 31: 721–731.

Tan, L.L., Oswald, M.J., Heinl, C. *et al.* (2019). Gamma oscillations in somatosensory cortex recruit prefrontal and descending serotonergic pathways in aversion and nociception. *Nat Commun.* 10: 983.

Tayeb, Z., Bose, R., Dragomir, A. *et al.* (2020). Decoding of pain perception using EEG signals for a real-time reflex system in prostheses: a case study. *Sci. Rep.* 10: 5606.

Tiemann L, Hohn VD, Ta Dinh S, May ES, Nickel MM, Gross J, Ploner M. (2018). Distinct patterns of brain activity mediate perceptual and motor and autonomic responses to noxious stimuli. *Nat. Commun*. 9: 4487.

Tu Y, Tan A, Bai Y, Hung Y S, Zhang Z (2016). Decoding subjective intensity of nociceptive pain from pre-stimulus and post-stimulus brain activities. *Front. Comp. Neurosci.* 10: 32.

Urien L, Xiao Z, Dale J, *et al.* (2018). Rate and temporal coding mechanisms in the anterior cingulate cortex for pain anticipation. *Sci. Rep.* 8: 8298.

van der Miesen, MM, Lindquist, MA, Wager, TD (2019). Neuroimaging-based biomarkers for pain: state of the field and current directions. *PAIN Reports* 4: e751.

Vierck CJ, Whitsel BL, Favorov OV, Brown AW, Tommerdahl M (2013). Role of primary somatosensory cortex in the coding of pain. *Pain* 154: 334-344.

Wager TD, Atlas LY, Lindquist MA, Roy M, Woo CW, Kross E (2013). An fMRI-based neurologic signature of physical pain. *N. Engl. J. Med*. 368: 1388-1397.

Xiao Z, Hu S, Zhang Q, Tian X, Chen W, Wang J, Chen Z (2019). Ensembles of change-point detectors: implications for real-time BMI applications. *J. Comput. Neurosci.* 46: 107-124.

Xiao Z, Martinez E, et al. (2019). Cortical pain processing in the rat anterior cingulate cortex and primary somatosensory cortex. *Front. Cell. Neurosci.* 13: 165.

Zhang Q, Xiao Z, Huang C, Hu S, Kulkarni P, Martinez E, Tong AP, Garg A, Chen Z, Wang J (2018). Local field potential decoding of the onset and intensity of acute pain in rats. *Sci. Rep*. 8: 1-11.

Zhang Q, Hu S, Talay R, Xiao Z, Rosenberg D, Li A, Caravan B, Liu Y, Sun G, Singh A, Gould JD, Chen Z, Wang J (2020). A closed-loop brain-machine interface for the study and treatment of pain. *Nat. Biomed. Eng.*, to appear.

Zhou R, Wang J, Qi W, Liu F-Y, Yi M, Guo H, Wan Y (2018). Elevated resting state gamma oscillatory activities in electroencephalogram of paitents with post-herpetic neuralgia. *Front. Neurosci.* 12: 750.

Zhang S, Yoshida W, Mano H, et al. (2020). Pain control by co-adaptive learning in a brain-machine interface. *Curr. Biol.* 30: 1-10.

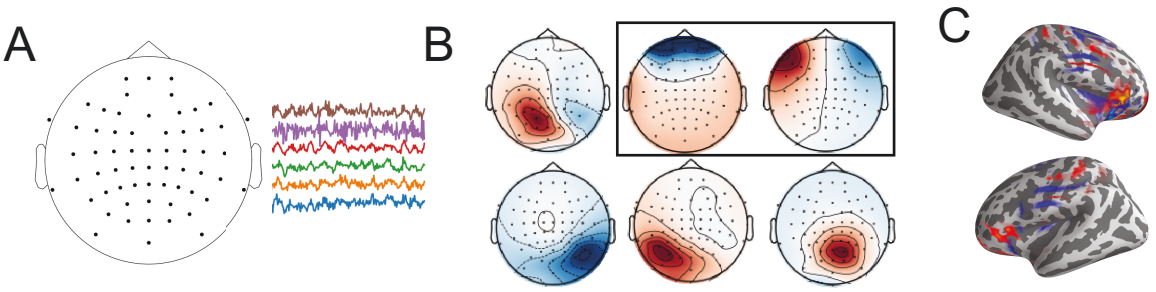

Figure 1. Schematic of EEG signal processing and source localization. **A:** Illustration of high-density EEG data acquisition. **B**: Independent component analysis (ICA) for rejection of eyeblink artifacts (two upper right components related to eye movement are indicated in the box). The warm (cold) color in scalp topography

indicates high (low) energy in the EEG. **C:** Illustration of localized sources on the cortical surfaces in two hemispheres. Warm color indicates high activation activity.

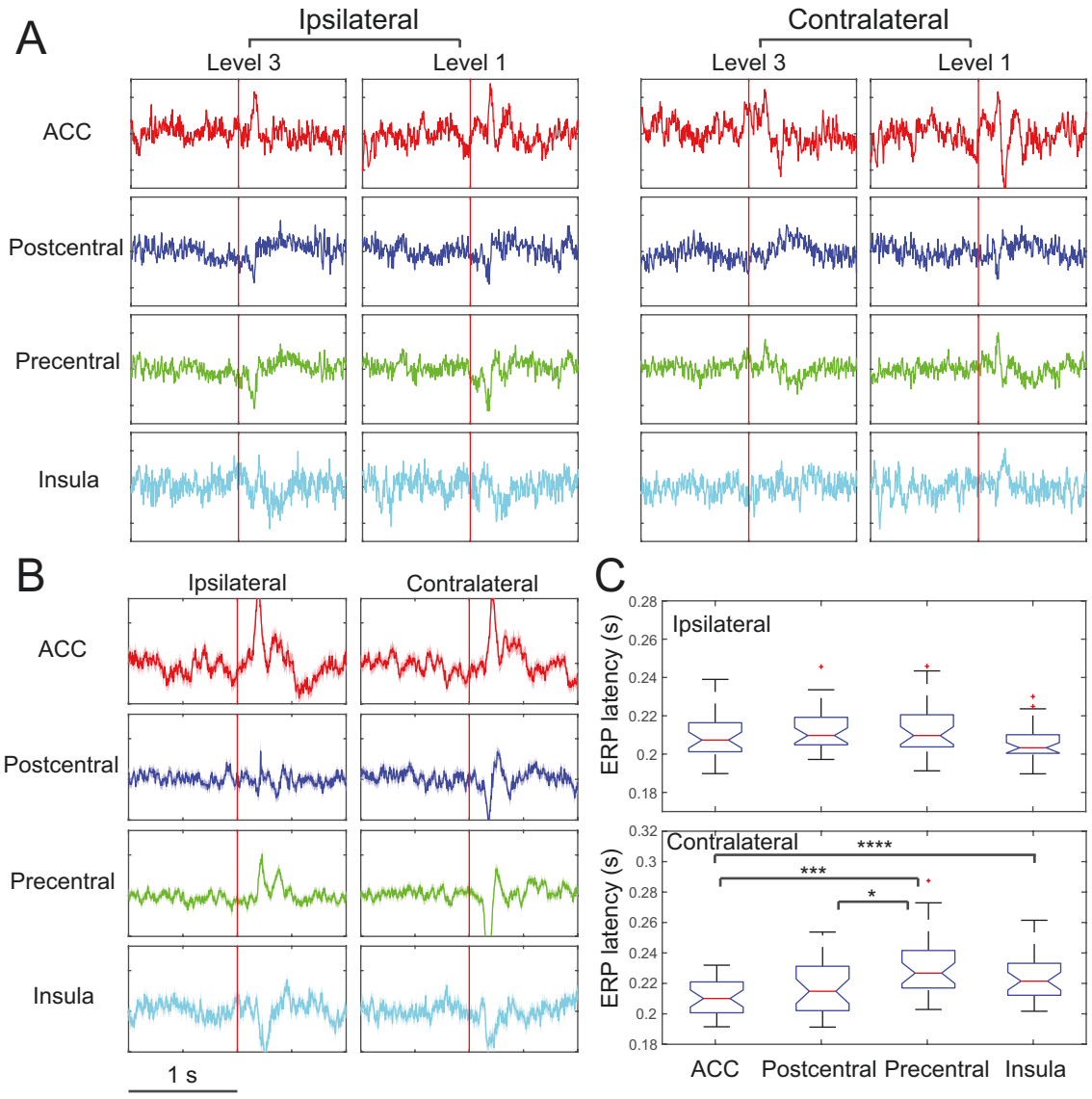

Figure 2. Results on event-related potentials (ERPs) upon EEG source localization. A: Representative single-trial ERPs from 8 ROIs upon EEG source localization. **B**: Trial-averaged ERPs from one representative subject. Shaded area represents standard error of mean (SEM). **C**: Group statistics of ERP latency at both ipsilateral and contralateral hemispheres (*, p<0.05; **, p<0.01; ***, p<0.001; ****, p<0.0001; rank-sum test).

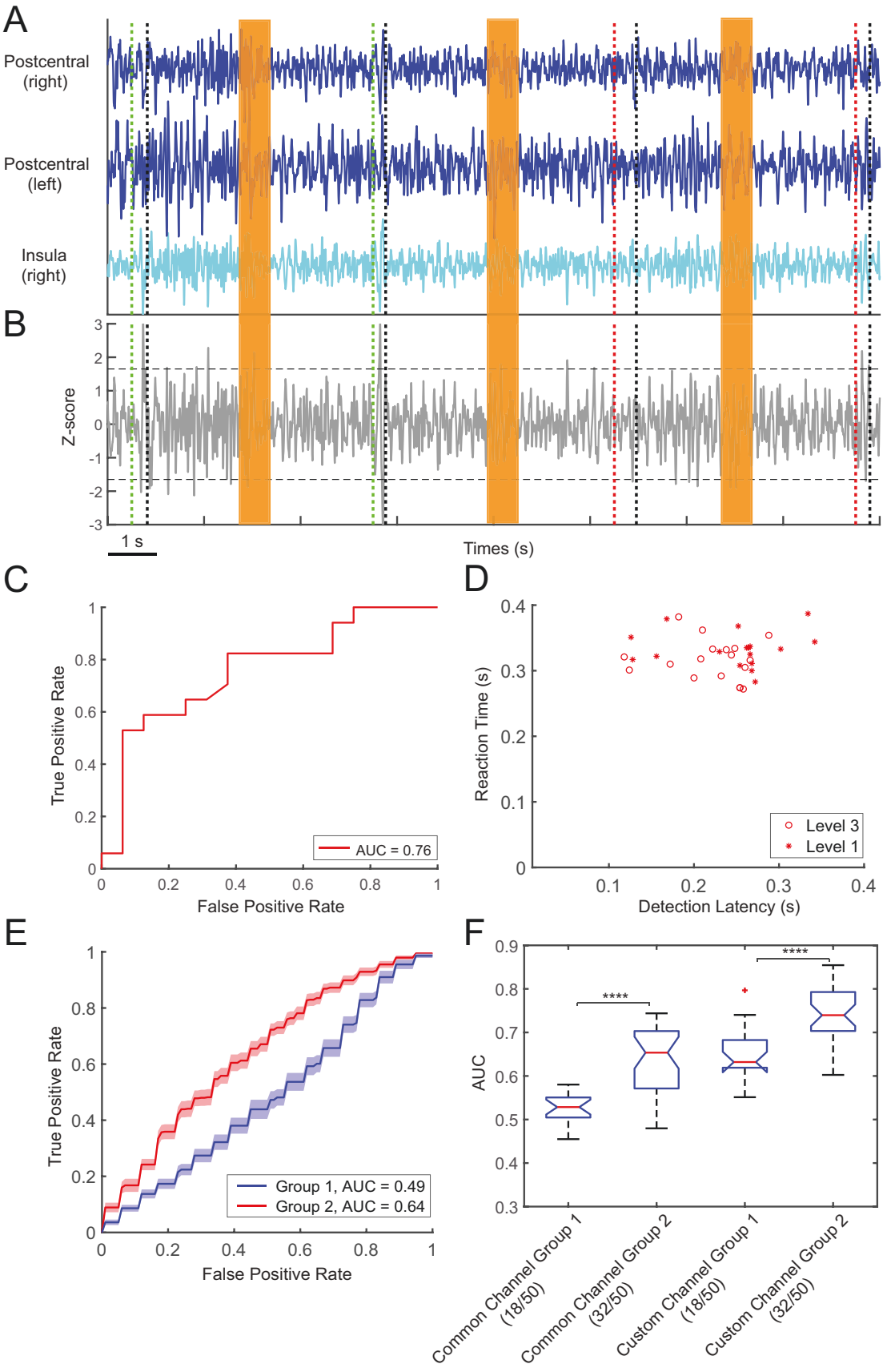
A
Postcentral (right)
Postcentral (left)
Insula (right)
B
Z-score
1 s
Times (s)
C
True Positive Rate
False Positive Rate
AUC = 0.76
D
Reaction Time (s)
Detection Latency (s)
Level 3
Level 1
E
True Positive Rate
False Positive Rate
Group 1, AUC = 0.49
Group 2, AUC = 0.64
F
AUC
****
****
Common Channel Group 1 (18/50)
Common Channel Group 2 (32/50)
Custom Channel Group 1 (18/50)
Custom Channel Group 2 (32/50)

Figure 3. Unsupervised methods for detecting acute pain signals. A: Representative snapshot of source-localized EEG traces from three ROIs (subject #1). The green and red vertical dotted lines represent the onset of randomly interleaved Level-3 and Leve-1 noxious stimuli, respectively; black vertical dotted lines represent the subject's reaction time. Orange shaded boxes represent the inter-trial periods that are not completely shown. **B:** Z-score trace derived from the SSM. Horizontal dashed lines represent the detection threshold of statistical significance. **C:** ROC curve derived from unsupervised detection for one representative subject. The area under the curve (AUC) was 0.76. **D:** Comparison between the detection latency of pain onset and subject's reaction time at the single-trial level showed weak yet non-significant correlation (Spearman's rank correlation ρ=0.29, p=0.06). **E:** Group-averaged ROC curves. The mean AUC statistics were 0.49 for Group 1 (n=18) and 0.64 for Group 2 (n=32)**. F:** Comparison of detection performance in AUC between Group 1 and Group 2, based on using either common ROI features for all subjects or customized ROI features for each subject. The AUC was greater in Group 1 than in Group 2, during both common (p=1.9×10^{-5}; rank-sum test) and subject custom selection (p=3.4×10^{-5}) settings.

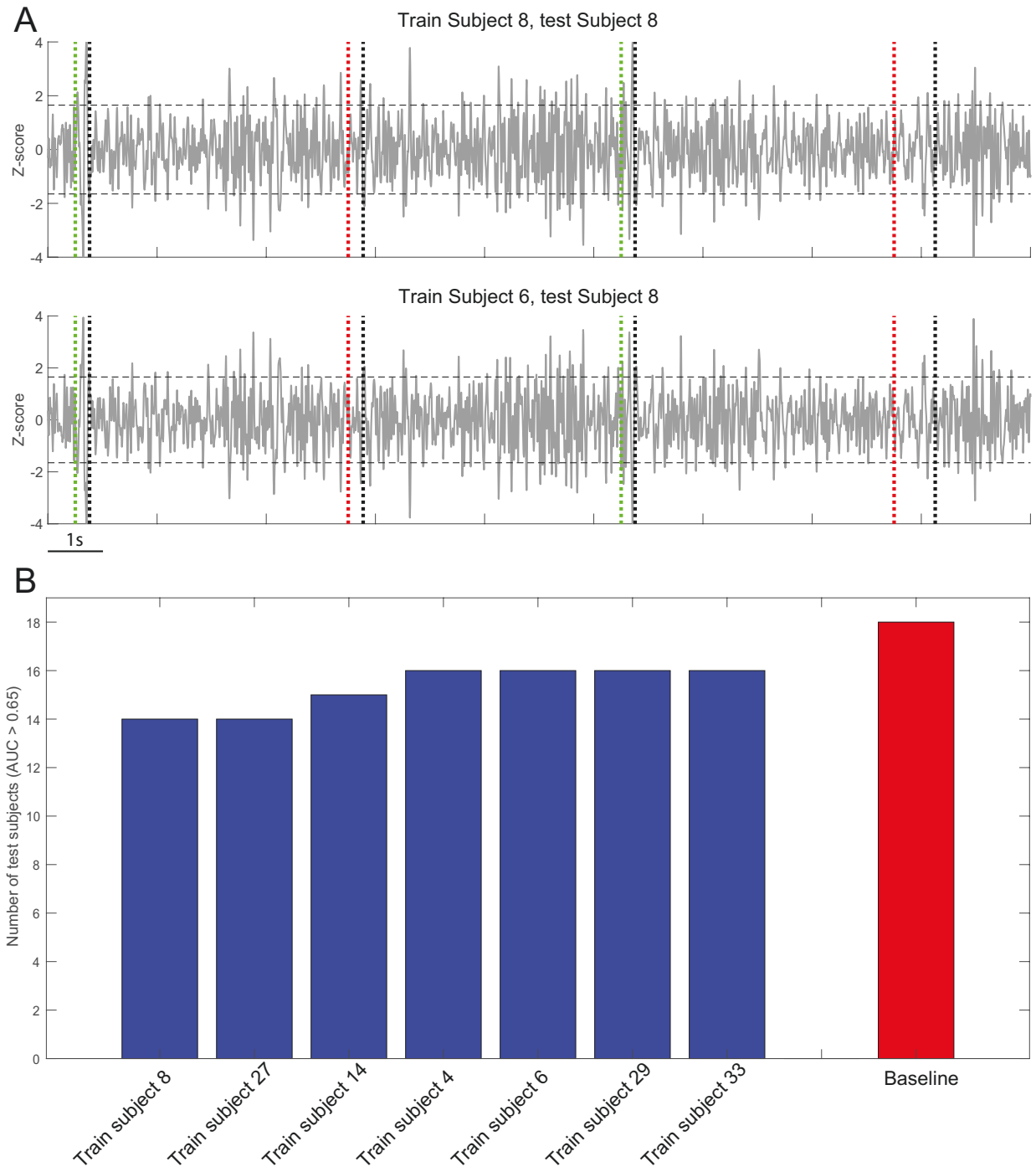

Figure 4. Cross-subject prediction for detecting acute pain signals. A: Z-score trace derived from the SSM. The green and red vertical dotted lines represent the onset of randomly interleaved Level-3 and Leve-1 noxious stimuli. Horizontal dashed lines represent the detection threshold of statistical significance. Top row: within-subject prediction; bottom row: cross-subject prediction. **B:** The number of tested subjects achieving >0.65 AUC in cross-subject prediction. The baseline is referred to within-subject prediction.

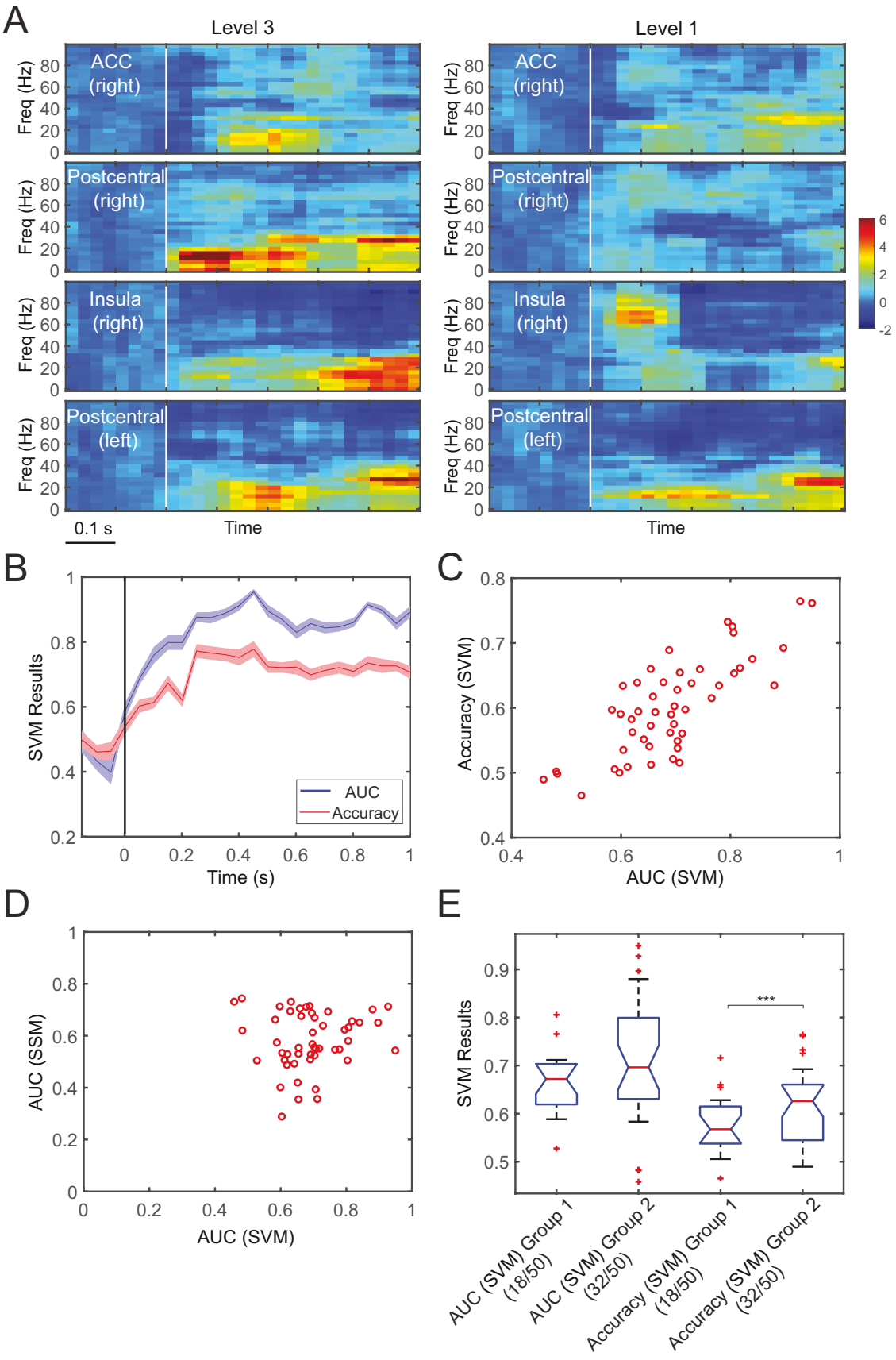
A
Level 3
Level 1
ACC (right)
Postcentral (right)
Insula (right)
Postcentral (left)
Freq (Hz)
0.1 s
Time
B
SVM Results
Time (s)
AUC
Accuracy
C
Accuracy (SVM)
AUC (SVM)
D
AUC (SSM)
AUC (SVM)
E
SVM Results
***
AUC (SVM) Group 1 (18/50)
AUC (SVM) Group 2 (32/50)
Accuracy (SVM) Group 1 (18/50)
Accuracy (SVM) Group 2 (32/50)

Figure 5. SVM for classifying acute pain signals. A: Comparison of trial-averaged Z-score source-localized EEG spectrograms from one representative subject, between Level-3 and Level-1 trials. **B:** Cumulative cross-validated decoding accuracy curve and ROC curve computed from the SVM analysis from one representative subject. The timing of peak performance was around 400 ms. **C:** Group statistics of peak detection accuracy and AUC, which are positively correlated (Pearson's correlation ρ=0.71, p=10^{-5}). **D:** Comparison of the AUC statistics derived from unsupervised SSM and supervised SVM methods. There was no significant correlation in AUC between two methods (Pearson's correlation ρ=0.08, p=0.56). **E:** Comparison of classification performance in peak accuracy and AUC between Group 1 (n=18) and Group 2 (n=32). There was a significant difference in accuracy between Group 1 and Group 2 (p=1.2×10^{-4}, rank-sum test).

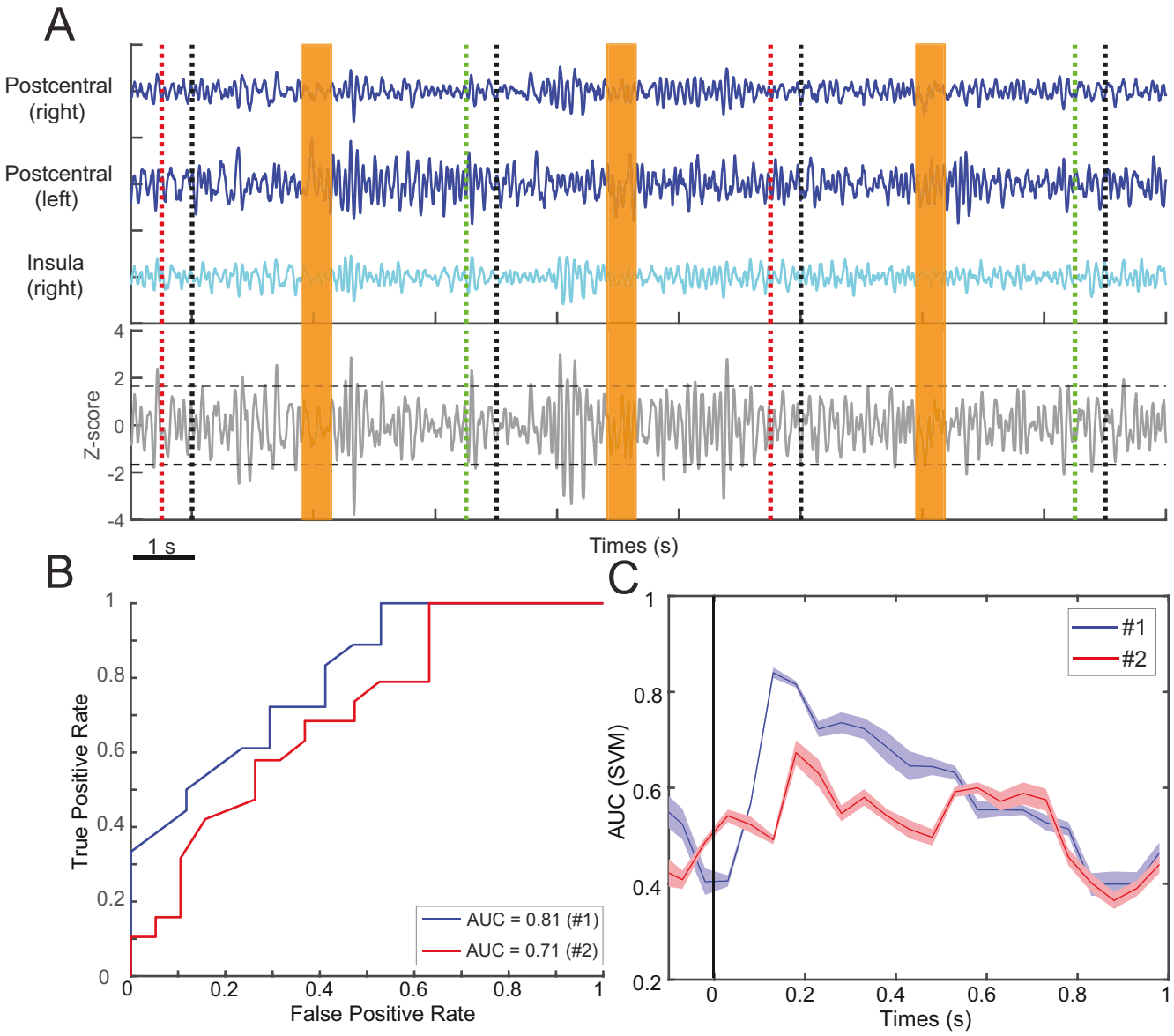

Figure 6. Pain detection results derived from two chronic pain patients. A: Representative snapshot of source-localized EEG traces from three ROIs and the pain detection Z-score trace derived from the SSM. The green and red vertical dotted lines represent the onset of randomly interleaved noxious and non-noxious stimuli, respectively. Orange shaded boxes illustrate the inter-trial periods that are not shown. Horizontal dashed lines represent the detection threshold of statistical significance. **B:** ROC curves derived from unsupervised detection in hand stimulations for two subjects. **C**: AUC curves derived from SVM classification in back stimulations for two subjects. The timing of peak performance was around 180-200 ms upon the stimulus onset (time 0).

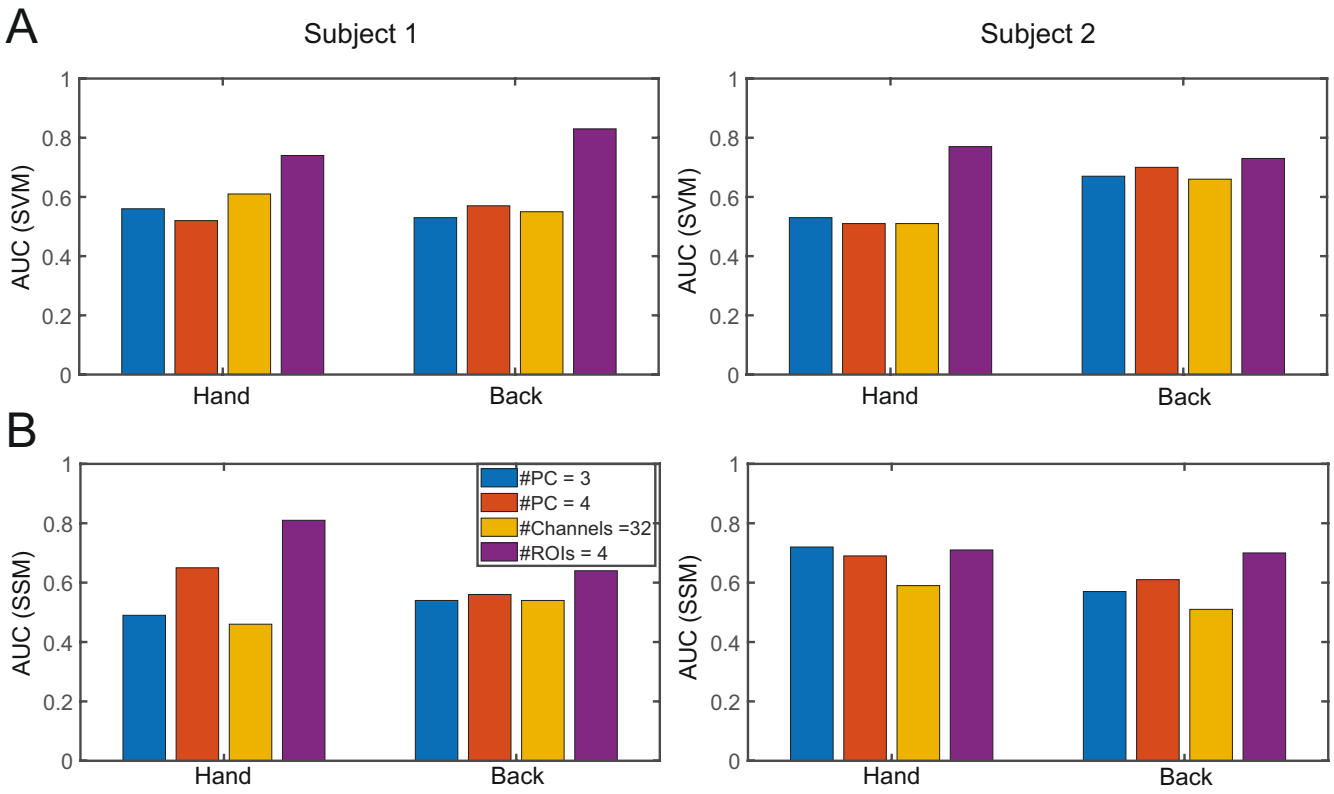

Figure 7. Performance comparison of pain detection results without EEG source localization. A: SVM results for two chronic pain patients. **B:** SSM-based detection results for two chronic pain patients. In all comparisons, PCA was conducted to keep 3-4 principal components (PCs) to match the number of selected ROIs used in source localization-based detection results. Overall, the results derived from EEG source localization showed the best AUC performance.